The EMBO Journal (2006) 25, 4338–4349 | © 2006 European Molecular Biology Organization | All Rights Reserved 0261-4189/06
www.embojournal.org

THE EMBO JOURNAL

Systems analysis of effector caspase activation and its control by X-linked inhibitor of apoptosis protein

Markus Rehm[1,3], Heinrich J Huber[2,3], Heiko Dussmann[1] and Jochen HM Prehn[1,*]

[1]Department of Physiology & Medical Physics, Royal College of Surgeons in Ireland, Dublin, Ireland and [2]Siemens Medical Division, Siemens Ireland, Dublin, Ireland

Activation of effector caspases is a final step during apoptosis. Single-cell imaging studies have demonstrated that this process may occur as a rapid, all-or-none response, triggering a complete substrate cleavage within 15 min. Based on biochemical data from HeLa cells, we have developed a computational model of apoptosome-dependent caspase activation that was sufficient to remodel the rapid kinetics of effector caspase activation observed *in vivo*. Sensitivity analyses predicted a critical role for caspase-3-dependent feedback signalling and the X-linked-inhibitor-of-apoptosis-protein (XIAP), but a less prominent role for the XIAP antagonist Smac. Single-cell experiments employing a caspase fluorescence resonance energy transfer substrate verified these model predictions qualitatively and quantitatively. XIAP was predicted to control this all-or-none response, with concentrations as high as 0.15 μM enabling, but concentrations >0.30 μM significantly blocking substrate cleavage. Overexpression of XIAP within these threshold concentrations produced cells showing slow effector caspase activation and submaximal substrate cleavage. Our study supports the hypothesis that high levels of XIAP control caspase activation and substrate cleavage, and may promote apoptosis resistance and sublethal caspase activation *in vivo*.
The EMBO Journal (2006) **25,** 4338–4349. doi:10.1038/sj.emboj.7601295; Published online 24 August 2006
Subject Categories: differentiation & death
Keywords: apoptosis; caspases; single-cell imaging; systems biology; XIAP

Introduction

Apoptosis removes superfluous or damaged cells from the body of multicellular organisms. Enhanced or repressed apoptotic cell death contributes to developmental defects, autoimmune diseases, cancer and neurological disorders (Meier *et al*, 2000; Yuan and Yankner, 2000). Activation of effector caspases is a central and ultimate step in many apoptosis pathways. In the intrinsic pathway, the activation of effector caspases is triggered by mitochondrial outer membrane permeabilisation (MOMP) and the subsequent release of proapoptotic proteins into the cytosol. The release of cytochrome *c* (cyt-*c*) triggers the formation of the apoptosome, a multiprotein complex comprising apoptotic protease-activating factor 1 (Apaf-1), procaspase-9, dATP/ATP and cyt-*c* (Li *et al*, 1997; Zou *et al*, 1997). Apoptosome-bound caspase-9 subsequently activates effector caspases-3 and -7 that are responsible for most of the morphological and biochemical changes occurring during this type of active cell death (Li *et al*, 1997; Zou *et al*, 1997; Janicke *et al*, 1998b; Slee *et al*, 1999). The signalling network gains complexity by additional caspase-3-dependent feedbacks (Slee *et al*, 1999).

The X-linked-inhibitor-of-apoptosis-protein (XIAP) is a cytosolic inhibitor of caspases-9, -3 and -7 and the most potent member of the IAP family of proteins (Deveraux and Reed, 1999). XIAP can be counteracted by the second mitochondria-derived activator of caspases (Smac)/DIABLO (Du *et al*, 2000; Verhagen *et al*, 2000). Smac is released from mitochondria together with cyt-*c* and competitively and sterically displaces caspases from their XIAP interaction sites (Wu *et al*, 2000; Rehm *et al*, 2003). XIAP also enforces the degradation of its binding partners by ubiquitination (Suzuki *et al*, 2001; MacFarlane *et al*, 2002). However, recent studies demonstrated a lack of phenotype in XIAP-deficient mice and human cells in response to the activation of the intrinsic apoptosis pathway and have questioned a significant role for XIAP in apoptosis regulation (Harlin *et al*, 2001; Wilkinson *et al*, 2004).

Single-cell imaging studies using fluorescence resonance energy transfer (FRET) probes containing conserved caspase cleavage sites have demonstrated that the activation of effector caspases during apoptosis may be a rapid, all-or-none process (Tyas *et al*, 2000; Rehm *et al*, 2002). We have previously also found that efficient effector caspase activation can occur within 5 min of MOMP (Rehm *et al*, 2003). Although these studies demonstrated an astonishing efficiency of the apoptotic signalling cascade, a comprehensive explanation for this rapid, all-or-none behaviour and its control by XIAP and factors such as Smac is still lacking. The complex nature of a protein network with multiple variables acting at the same time can only be analysed on a systems level. We therefore have developed a computational model of the process of apoptosome-dependent caspase activation based on a 53 reactions network that enabled us to study, understand and subsequently experimentally verify effector caspase activation and its control by XIAP.

Results

Computational modelling and single-cell analysis of apoptosome-dependent effector caspase activation in HeLa cells

We developed a computational model of apoptosome-dependent effector caspase activation in HeLa cells. In this

*Corresponding author. Department of Physiology & Medical Physics, Royal College of Surgeons in Ireland, 123 St Stephen's Green, Dublin 2, Ireland. Tel.: +353 1 402 22 55; Fax: +353 1 402 22 61;
E-mail: prehn@rcsi.ie
[3]These authors contributed equally to this work

Received: 22 December 2005; accepted: 1 August 2006; published online: 24 August 2006

 ©2006 European Molecular Biology Organization

computational approach, cyt-*c* and Smac release initiate a reactions network that eventually leads to the activation of effector caspases. A full description of the model is provided as Supplementary data 1. The model was implemented in MATLAB and integrates known and *de novo*-determined protein concentrations (Supplementary data 2), reaction, degradation and inhibitory constants, as well as the individual kinetics for cyt-*c* release, Smac release, and the cyt-*c*-induced apoptosome formation. The resulting substrate cleavage serves as an output function (Figure 1A). The model was *a priori* designed to allow a direct comparison of the model output with the cleavage of an FRET-based effector caspase substrate in single-cell imaging experiments, allowing a validation of model predictions.

In vivo responses were recorded in HeLa cells exposed to the kinase inhibitor staurosporine (STS), a stimulus that induces cell death through the mitochondrial apoptosis pathway (Tafani *et al*, 2001; Rehm *et al*, 2002). The onset of MOMP in response to STS was determined *in vivo* using tetramethylrhodamine methylester (TMRM), a fluorescent probe used to measure fast changes in the mitochondrial membrane potential ($\Delta\Psi_M$). The release of cyt-*c* occurs concomitantly with $\Delta\Psi_M$ depolarisation and the loss of cyt-*c* causes this initial depolarisation, as readdition of cyt-*c* is able to restore $\Delta\Psi_M$(Varnes *et al*, 1999; Dussmann *et al*, 2003; Rehm *et al*, 2003; Goldstein *et al*, 2005). Effector caspase-dependent substrate cleavage was detected by FRET analysis using a recombinant CFP-DEVD-YFP fusion protein (Tyas *et al*, 2000; Rehm *et al*, 2002). In HeLa cells stably expressing the FRET probe, effector caspase activation in response to 1 μM STS manifested rapidly after the onset of MOMP (Figure 1B and C). In agreement with previous findings from our group (Rehm *et al*, 2003), quantitative analysis of the imaging data revealed an average time window of 4 min between MOMP and effector caspases activation (Figures 1C and 4F), and a complete cleavage of the FRET substrate within 15 min (Figure 1D).

Temporal protein profiles during apoptosome-dependent effector caspase activation

Analysis of effector caspase activation using the above-described computational model produced an output that very closely resembled the biological responses observed in the single-cell imaging experiments (Figure 2A). Modelling of effector caspase-dependent substrate cleavage calculated an onset of effector caspase activation ~5 min after cyt-*c* release, reaching completion after 15 min.

The model subsequently allowed us to calculate and illustrate changes in protein concentrations and interactions over time, providing insights into the kinetics of the underlying signalling process (Figure 2B–F). Following cyt-*c* release, apoptosome formation and Smac release (Figure 2B), active caspase-9 (p35/p10) is generated shortly before a pronounced increase in active caspase-3 (Figure 2C). The temporal relationship of these events suggests a tight coupling of both processes. This can be explained by the caspase-3-dependent feedback on the apoptosome which generates the caspase-9 (p35/p10) form (Srinivasula *et al*, 2001). Caspase-9 (p35/p10) has an increased enzymatic activity when compared to caspase-9 (p35/p12) and cannot be inhibited by XIAP (Srinivasula *et al*, 2001; Zou *et al*, 2003). Therefore, caspase-3 can sharply increase as soon as a substantial amount of caspase-9 (p35/p10) has been generated.

The model predicts that free XIAP levels rapidly decrease during the first 10 min following the onset of cyt-*c* release (Figure 2D). About 35% of the total XIAP binds to the apoptosome-associated caspase-9 (p35/p12), peaking at ~6 min. XIAP also rapidly inhibits caspase-3 with a steady increase peaking at ~10 min. The model predicts that the p2 fragment, also termed decoy peptide, generated by processing caspase-9 (p35/p12) to the p35/p10 form only plays a minor role as it is never present in sufficient amounts to substantially block XIAP (Figure 2D). Significant caspase-3-dependent cleavage of XIAP sets in 10 min after cyt-*c* release, generating the BIR1-2 and BIR3-RING fragments (Figure 2E). The majority of the BIR1-2 fraction binds to and inhibits caspase-3, whereas the BIR3-RING fraction is predominantly free in the cytosol or bound to the p2 fragment of caspase-9 (Figure 2E).

Following its release into the cytosol, Smac binding to XIAP peaks 8 min after the onset of MOMP. Surprisingly, only about 10% of the total Smac protein can bind to XIAP before XIAP cleavage sets in, suggesting that Smac might only play a minor role at standard physiological conditions (Figure 2F). Owing to the low affinity, Smac binding to XIAP cleavage products plays no significant role (data not shown).

Modelling of the effects of caspase and proteasome inhibition on cytosolic Smac/DIABLO levels

Smac is released together with cyt-*c* after MOMP (Rehm *et al*, 2003). Caspase inhibition with the broad-spectrum caspase inhibitor zVAD-fmk decreases cytosolic Smac levels significantly (Rehm *et al*, 2003; Sun *et al*, 2004). However, cytosolic Smac levels can be restored by the addition of proteasome inhibitors, suggesting that proteasome-dependent Smac degradation is accelerated under conditions of caspase inhibition (MacFarlane *et al*, 2002; Rehm *et al*, 2003; Sun *et al*, 2004). To provide a mathematical explanation for these findings, caspase activities or protein degradation constants in the model were set to zero and cytosolic Smac levels were modelled (Figure 2G). Caspase inhibition resulted in a significant degradation of cytosolic Smac, whereas proteasome inhibition kept Smac protein levels at a consistently high level. The model explains the enforced Smac degradation by the zVAD-fmk-inhibited caspase fraction, resulting in a higher amount of free XIAP. XIAP in turn binds to Smac, enforcing Smac degradation by ubiquitination. In addition, caspase-dependent cleavage of the proteasome is blocked and Smac degradation therefore prevails through the later stages of apoptosis (Figure 2G).

Sensitivity analysis predicts an XIAP-dependent threshold for effector caspase activation

To identify the key parameters affecting caspase activation, we analysed how the model responded to changes in protein concentrations and alterations in the kinetics of the input functions. Responses were evaluated by the time required to cleave 20 or 80% of the caspase substrate after the onset of MOMP (Figure 3A–F). At standard conditions (defined as conditions in naïve HeLa cells), 20% of the substrate was cleaved by 8 min, and 80% by 12 min after MOMP. Surprisingly, altering the kinetics of cyt-*c*-induced apopto-

©2006 European Molecular Biology Organization

some formation or Smac release only slightly affected the substrate cleavage, and fast effector caspase activation persisted even when kinetics were significantly slowed down (Figure 3A and B). Alterations in the Smac concentration also only had a minor influence on substrate cleavage (Figure 3C). In HeLa cells, apoptosome formation is quantitatively limited by the amount of procaspase-9 (Supplementary data 2). As expected, substrate cleavage was highly sensitive to changes in procaspase-9 and procaspase-3 concentrations, with potent inhibition of substrate cleavage at subphysiological concentrations (Figure 3D–E). In other cell types, the amount of Apaf-1 may limit apoptosome formation. In such cases, the system would respond with sensitivities to altered Apaf-1 concentrations that correspond to those observed for procaspase-9 in the HeLa model.

In agreement with previous studies that demonstrated levels of apoptosis were not altered in XIAP-deficient animals (Harlin *et al*, 2001), lowering the physiological XIAP concentration did not significantly accelerate substrate cleavage after the onset of MOMP (Figure 3F). Elevated XIAP protein levels, however, delayed substrate cleavage exponentially (Figure 3F), suggesting that high XIAP concentrations may fully block caspase activation.

To study this phenomenon in more detail, we plotted substrate cleavage profiles for a continuous range of XIAP concentrations from 0 μM (knockout) to 0.5 μM (eightfold higher than the physiological concentration in naïve HeLa cells) (Figure 4A). Interestingly, the computational analysis predicted that XIAP concentrations between 0.15 and 0.30 μM separate conditions of complete substrate cleavage from conditions that lack significant substrate cleavage.

Single-cell analysis in XIAP overexpressing cells confirms model predictions

To confirm these model predictions, we tested the effect of XIAP overexpression on effector caspase activation in real-time. HeLa cells were infected with an XIAP expression adenovirus (AdV-XIAP) (multiplicity of infection (m.o.i.) 100) and apoptosis was induced with 1 μM STS. Western blotting confirmed a strong XIAP overexpression following adenoviral infection (Figure 4B). Subsequent densitometry analysis revealed that the XIAP protein level in AdV-XIAP-infected cultures was 4.5 times higher than the protein level under control conditions. As the physiological XIAP concentration in HeLa cells has been determined as 0.063 μM, adenovirus-mediated overexpression of XIAP hence should fall within the predicted XIAP concentration threshold ($4.5 \times 0.063\ \mu M = 0.28\ \mu M$).

Single-cell imaging revealed that cells overexpressing XIAP indeed showed a pronounced delay between MOMP and effector caspase activation (Figure 4C; compare to Figure 1B). Modelled substrate cleavage kinetics around a XIAP concentration of 0.28 μM calculated slower cleavage kinetics and submaximal substrate cleavage (Figure 4D). Correspondingly, individual traces of HeLa cells infected with AdV-XIAP showed submaximal substrate cleavage and substantially altered activation kinetics, very closely resembling the model predictions (Figure 4E).

Quantitative analysis indicated that the delay between MOMP and effector caspase activation increased from 4 min in noninfected or AdV-LacZ-infected controls to 12 min in AdV-XIAP-infected HeLa cells (Figure 4F). Quantitative analysis of substrate cleavage durations using a sigmoid Boltzmann function likewise demonstrated reduced caspase activity in XIAP-overexpressing cells (Figure 4G). In these calculations, the width of the sigmoid turnover was determined by the factor d*t* and was used as a measure for the duration of substrate cleavage (Rehm *et al*, 2002). Because the adenovirus-mediated overexpression of XIAP fell within the predicted XIAP threshold range, small cell-to-cell variations of XIAP levels *in vivo* should have a strong influence on the substrate cleavage characteristics of individual cells (compare with Figure 4A). This was clearly reflected by the higher variation of the 'time to cleavage' and 'width of turnover' values in the AdV-XIAP-infected cells compared to the control cells (Figure 4F and G).

Interestingly, 64% of cells that showed less than 40% substrate cleavage ($n = 11$ cells), and 78% of cells that showed less than 30% substrate cleavage ($n = 9$ cells) failed to develop morphological changes typical of apoptosis (shrinkage, blebbing) during the duration of the experiment. Below a threshold of 25% substrate cleavage, submaximal effector caspase activation failed to elicit an apoptotic phenotype in all cells investigated (15 h follow-up after MOMP).

Single-cell analysis in Smac-overexpressing cells confirms model predictions

The model predicted that variations in the Smac concentrations only mildly influence substrate cleavage (Figures 5A and 3C). We therefore experimentally examined the consequence of Smac overexpression on effector caspase activity in HeLa cells overexpressing Smac. HeLa cells were generated that exhibited a 3.4-fold overexpression of Smac, equalling an intracellular concentration of 0.428 μM (Supplementary data 2). Confirming the model predictions, substrate cleavage in these cells was not significantly accelerated compared to control HeLa cells (Figure 5B).

Figure 1 Modelled signalling network and cellular responses during apoptosome-dependent apoptosis. (**A**) Schematic representation of the modelled interaction network. Mitochondria undergo MOMP and concurrently depolarise. Following Apaf-1 oligomerisation and caspase-9 activation, effector caspases-3 and -7 get activated. Enzymatic cleavage processes are shown as green arrows; inhibitory interactions by XIAP and Smac proteins are shown as red dashed lines. Parameters in grey boxes serve as input and output functions of the computational model. Asterisks highlight reactions that are solely caspase-3 dependent. In addition, all proteins are subject to proteasomal degradation. (**B**) MOMP is followed by effector caspase activation. Images illustrate a representative HeLa cell infected with a β-galactosidase expression virus (AdV-LacZ; m.o.i. 100) and treated with 1 μM STS. Mitochondrial depolarisation is shown as a decrease in TMRM fluorescence. Cell boundaries are outlined in white. Time stamps show the time after stimulus addition. Effector caspase activation was detected by an increase in the CFP/YFP emission ratio because of proteolytical cleavage of a CFP-DEVD-YFP fusion protein (see Materials and methods). Probe cleavage in the cytosol precedes cleavage in nuclear regions. Scale bar = 5 μm. (**C**) Microscopy images were quantitatively analysed. Mitochondrial depolarisation (TMRM intensity) and effector caspase-dependent FRET disruption (CFP/YFP emission ratio) data for a representative HeLa cell is shown as function of time after stimulus addition (1 μM STS). Arrows indicate onset of depolarisation and onset of substrate cleavage. (**D**) Analysis of substrate cleavage. Traces from three representative HeLa cells show that FRET substrate cleavage during STS-induced apoptosis is complete. Traces were synchronised to the time point of depolarisation.

 ©2006 European Molecular Biology Organization

All-or-none caspase activation relies on positive feedback signalling

Caspase-3 orchestrates the final stages of apoptotic cell death by cleaving many characteristic caspase substrates. In addition, caspase-3 also positively feeds back onto the apoptosome by generating caspase-9 (p35/p10), which is believed to amplify signal progression (Zou *et al*, 2003). In this context, the model predicts that even very low pro-caspase-3 concentrations (~0.05 μM, compare with HeLa pro-caspase-3 concentration of 0.12 μM) are sufficient for

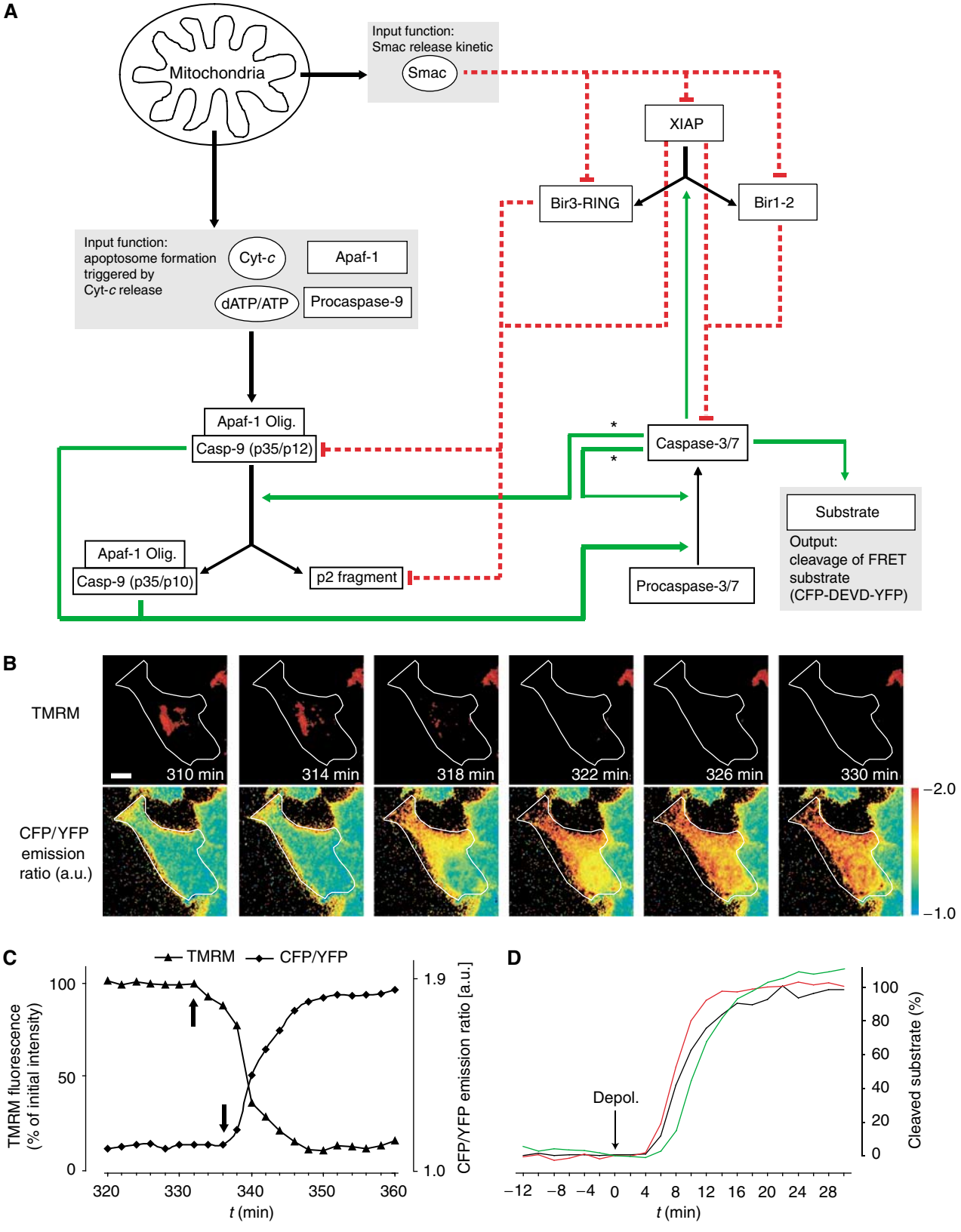

©2006 European Molecular Biology Organization

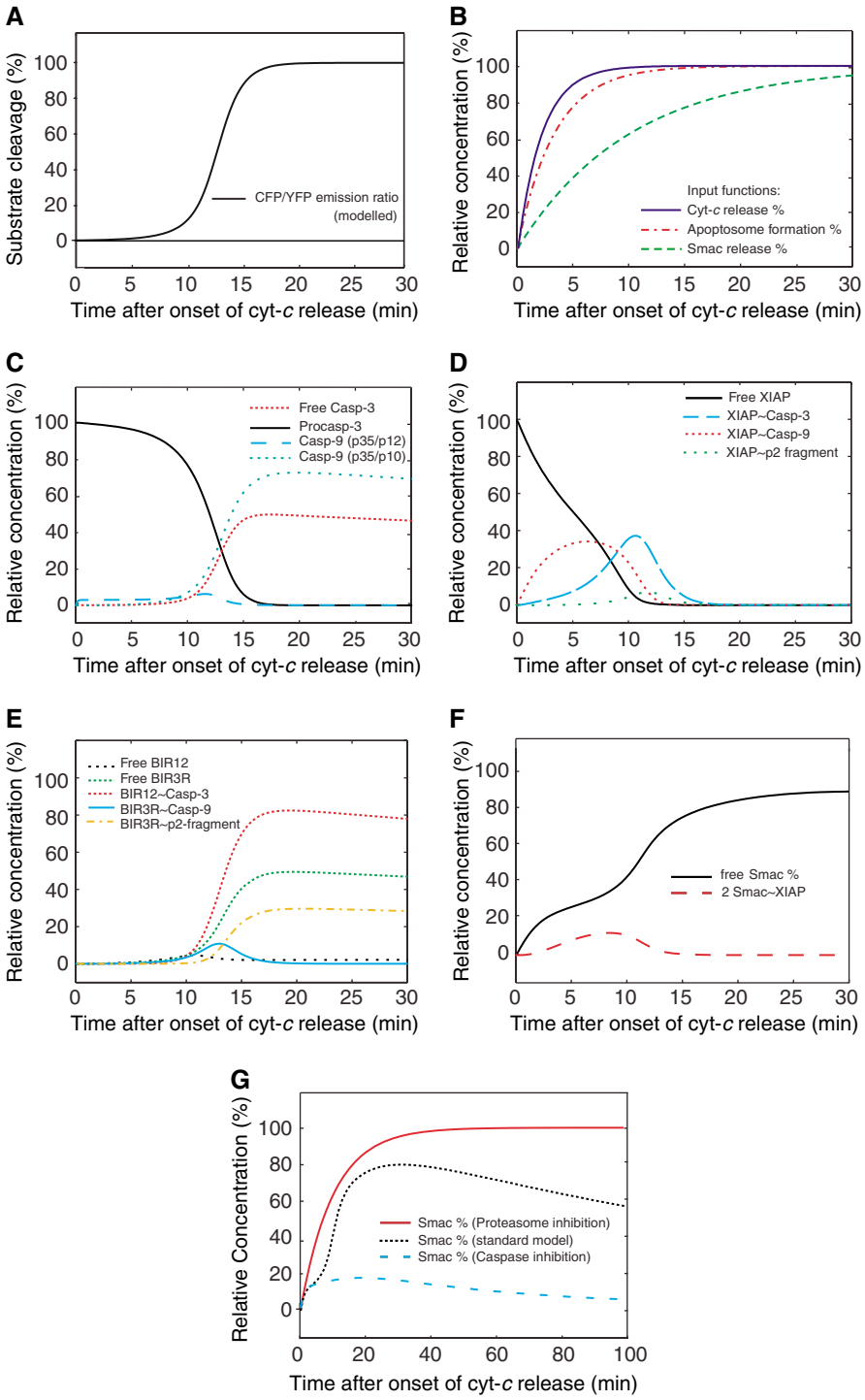

Figure 2 Protein profiles during apoptosome-dependent apoptosis. (**A**) Modelled output signal for the cleavage of an effector caspase FRET substrate under standard conditions. This model output can directly be compared to the experimental output (Figure 1C). (**B, C**) Cyt-*c* release, apoptosome formation and Smac release as model inputs lead to activation of apoptosome-bound caspase-9 and free caspase-3 (caspase-3 that is not inhibited by XIAP or BIR1-2). All concentrations are shown in relative units normalised to their potential maximum. (**D**) The amounts of free and caspase-bound XIAP fractions are shown normalised to the initial XIAP concentration. (**E**) The free XIAP cleavage products BIR1-2 and BIR3-RING, and the fractions bound to caspases are shown normalised to the initial XIAP concentration. (**F**) Free and XIAP-associated Smac is shown over time normalised to the initial XIAP concentration. (**G**) Modelled effects of proteasome and caspase inhibition on the Smac concentration. Proteasome inhibition prevents Smac degradation whereas inhibition of caspases by broad-spectrum caspase inhibitor z-VAD-fmk leads to an enforced Smac degradation.

rapid effector caspase activation and substrate cleavage (Figure 6A and C).

In caspase-3-deficient cells, a high expression level of caspase-7 may partly substitute for caspase-3. However, these cells still lack this caspase-3-dependent positive feedback loop (Slee *et al*, 1999). To understand how cells can compensate for the loss of caspase-3, caspase-3 and caspase-3-dependent feedback loops were eliminated from the HeLa model,

 ©2006 European Molecular Biology Organization

and effector caspase activity was adjusted to values for caspase-7 (i.e. we assumed that caspase-7 was the only effector caspase activated). Under these circumstances, the procaspase-7 concentration required for complete substrate cleavage was ~3-fold higher than for procaspase-3 in the standard model (Figure 6B and D). Indeed, it has been shown that caspase-3-deficient MCF-7 cells capable of undergoing apoptosis express elevated amounts of procaspase-7 (Janicke *et al*, 1998a). Of note, even at high procaspase-7 concentrations only ~35% of the initial protein was available as free effector caspase, and substrate cleavage was delayed and slow (Figure 6B and D). These results demonstrate that in the absence of caspase-3 strict all-or-none caspase activation is not achieved but substantial substrate cleavage is still possible.

We next modelled the role of XIAP in the two scenarios. In presence of caspase-3, XIAP concentrations that greatly exceed physiological conditions can lead to incomplete substrate cleavage (Figure 6E). However, in absence of caspase-3, the model predicts that slight overexpression of XIAP may be sufficient to block substrate cleavage completely (Figure 6F).

Lack of caspase-3 feedback signalling amplifies XIAP effects

From this model prediction, we hypothesised that in cells lacking the caspase-3 feedback loop, apoptosome-dependent effector caspase activation should be very efficiently inhibited by XIAP overexpression. Furthermore, this effect is expected to be so robust that it should also be detectable qualitatively in other cellular systems. To verify this, we used the well-established model system of caspase-3-deficient MCF-7 breast carcinoma cells. MCF-7 cells with the caspase-3 gene stably reintroduced (MCF-7/C3) served as an additional control.

In agreement with previously published data (Rehm *et al*, 2002, 2003), both MCF-7 and MCF-7/C3 cells underwent effector caspase activation after MOMP, but the loss of caspase-3 significantly extended the time between mitochondrial depolarisation and effector caspase activation (Figure 6G) and also reduced effector caspase activity (data not shown). A delayed response was also observed in MCF-7/C3 cells overexpressing XIAP by adenoviral infection (m.o.i. 100) (Figure 6G). However, the most pronounced phenotype was observed in MCF-7 cells overexpressing XIAP (100 m.o.i.), with >90% of cells showing a complete inhibition of substrate cleavage during the time course of the experiments (22 h) (Figure 6H).

Discussion

Cellular life/death decisions may require a robust decision matrix, both upstream and downstream of mitochondria. In the mitochondrial apoptosis pathway, effector caspase activation is initiated by the release of cyt-*c* from mitochondria (Zou *et al*, 1997). The initiating cyt-*c* release has been described to be a rapid all-or-none process (Goldstein *et al*, 2000). We demonstrate here qualitatively and quantitatively

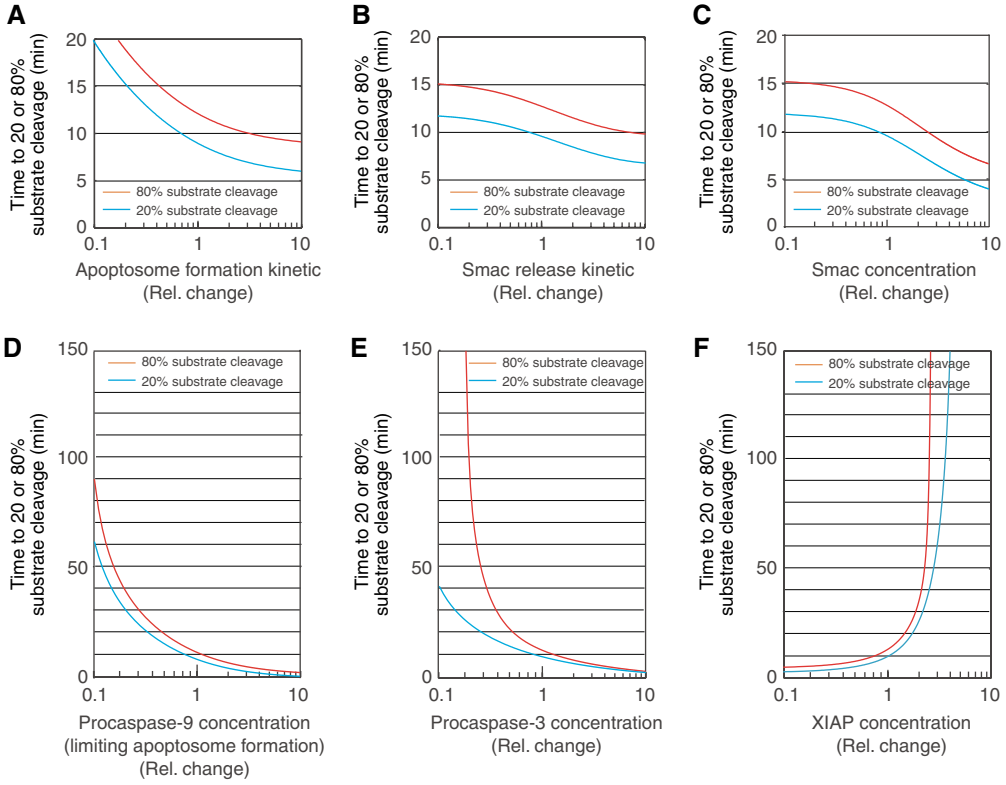

Figure 3 Sensitivity analysis predicts key players of apoptosome-dependent signalling. Selected parameters were varied independently from the others by up to two orders of magnitude around the standard value. The influence of the parameter variation on the output signal was investigated by calculating the time required for 20 and 80% substrate cleavage by effector caspases. (**A–C**) Variation of the cyt-*c* induced apoptosome formation and Smac release kinetics (time for 50% completion) or the Smac concentration have minor influences on the time required for substrate cleavage. (**D–F**) Decreasing the procaspase-9 or procaspase-3 concentrations, or increasing the XIAP concentration significantly delays the time required for substrate cleavage.

©2006 European Molecular Biology Organization

that the subsequent caspase activation network guarantees a swift execution of apoptosis. Interestingly, sensitivity analyses predicted that effector caspase activation may only mildly depend on the cyt-*c* release and subsequent apoptosome formation kinetics. This would argue against a biological role of any feedback of caspases on the mechanism of MOMP, as demonstrated in previous studies (Arnoult *et al*, 2003; Rehm *et al*, 2003; Ricci *et al*, 2004). This relative insensitivity can be explained by the fact that cyt-*c* has been shown to be present in excess when compared to

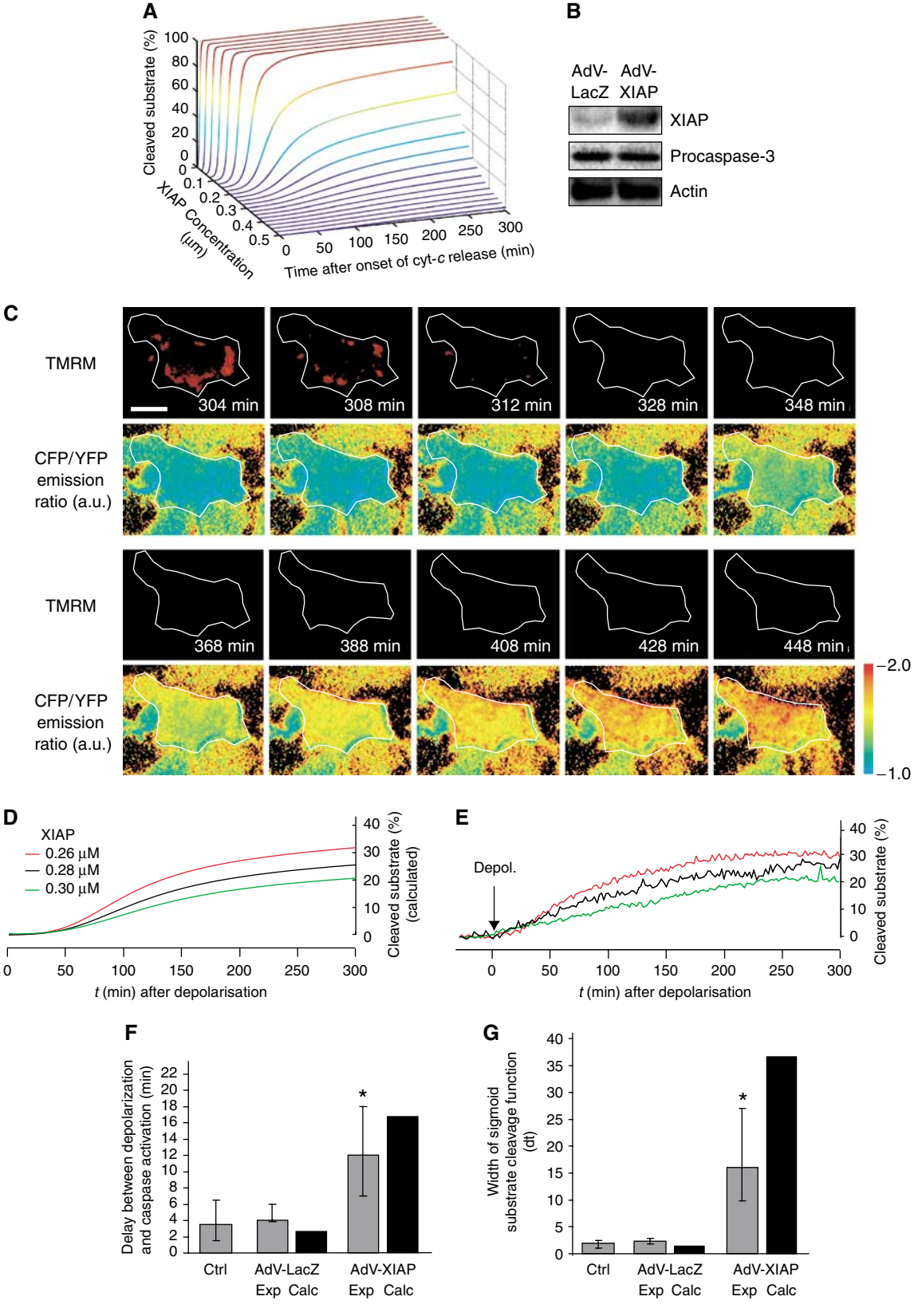

©2006 European Molecular Biology Organization

Apaf-1 or procaspase-9, and that either Apaf-1 or procaspase-9 stoichiometrically limit apoptosome formation. However, scenarios may exist where cyt-*c* levels are also rate-limiting, as a cyt-*c* threshold has recently been described in human T-cell leukemia cells (Murphy *et al*, 2003).

In addition to an important role of procaspase-9, Apaf-1 and caspase-3 described in previous studies (Kuida *et al*, 1996, 1998; Yoshida *et al*, 1998) and confirmed in the present study, we provide evidence for a critical role of XIAP in this system. Recent studies have demonstrated a lack of phenotype in both Smac- and XIAP-deficient mice, as well as in XIAP-deficient human cells during the activation of the mitochondrial apoptosis pathway (Harlin *et al*, 2001; Okada *et al*, 2002; Wilkinson *et al*, 2004). Our model predicts that these proteins are indeed redundant under physiological conditions. An interesting difference was, however, predicted in the respective overexpression scenarios. Smac overexpression was predicted to have little effect on effector caspase activation, a finding that was experimentally verified in subsequent single-cell studies. In contrast, overexpression of XIAP was predicted and experimentally verified to dramatically inhibit this process. This finding supports previous observations that elevated IAP levels can prevent apoptosis in resistant and malignant tumours (Tamm *et al*, 2000; Kashkar *et al*, 2003), and that XIAP may contribute to oncogenesis (Vaughan *et al*, 2002). In cells expressing high levels of XIAP, Smac however may become a second important player. Administration of Smac or Smac mimicking peptides can potentiate susceptibility to apoptosis-inducing agents in XIAP-expressing cells (Arnt *et al*, 2002; Li *et al*, 2004). Similarly, high XIAP concentrations have been shown to protect differentiated neuronal cells from apoptotic stimuli, and Smac injection is able to re-establish full responsiveness (Potts *et al*, 2003). Sensitivity analysis of the effects of combinations of high Smac and XIAP levels on effector caspase activation can confirm this model qualitatively and quantitatively (Supplementary data 3). It has also been suggested that nonlethal caspase activation is a frequent physiological process and may play an important role in cellular signal transduction (Sordet *et al*, 2002; Arama *et al*, 2003; Clarke *et al*, 2003; Weber and Menko, 2005). Taken together, our study suggests that (i) the positive feedback loop between caspase-9 and -3 and (ii) XIAP acting as a potentiometer on the kinetics of this feedback control the system's response during apoptosome-dependent apoptosis, and (iii) that submaximal substrate cleavage has a low probability to occur *in vivo*.

Interestingly, this study also provides preliminary information on how much caspase activity or substrate cleavage may be tolerated in cells without the subsequent appearance of a caspase-dependent apoptotic phenotype. Within the limitations of single-cell analyses and our FRET substrate approach, we provide here evidence that submaximal substrate cleavage (less than 25% in our experimental setting) does not elicit significant morphological changes in HeLa cells. Conversely, we found that all cells that exhibited greater than 65% substrate cleavage subsequently underwent apoptosis (data from $n=40$ cells). This finding highlights the requirement of an efficient effector caspase activation for the execution of apoptosis.

The 53 reaction network model that was based on ordinary differential equations provided us with detailed insight into the complex nonlinear signalling processes during apoptosome-dependent apoptosis. Previous systems biology studies have provided insights into the mechanisms of caspase activation in response to an activation of death receptors (Bentele *et al*, 2004; Eissing *et al*, 2004), however, largely bypassing the mitochondrial apoptosis pathway. Our study was also designed to avoid drawbacks of exclusive *in silico*

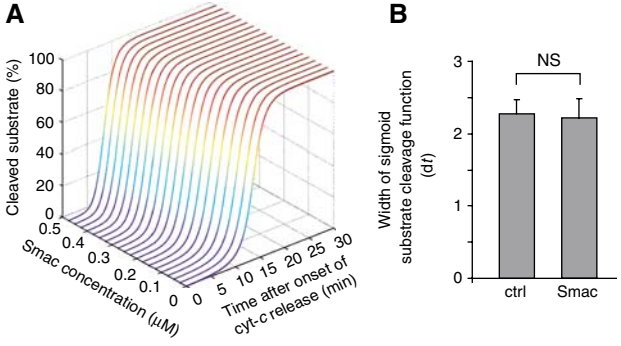

Figure 5 Smac overexpression does not accelerate substrate cleavage kinetics in HeLa cells. (**A**) Model prediction that increases in Smac concentration do not substantially alter substrate cleavage kinetics. (**B**) Evaluation of FRET substrate cleavage kinetics in single HeLa cells overexpressing Smac. Substrate cleavage traces for single cells were fitted with a sigmoid Boltzmann function. d*t* determines the width of the turnover of the sigmoid function. Data from $n=20$ or 19 cells are shown as mean + s.e.m. ($P=0.97$; *U*-test).

Figure 4 XIAP overexpression significantly decelerates apoptotic signalling and inhibits effector caspase activity. (**A**) A continuous variation of the XIAP concentration reveals a threshold between 0.15 and 0.30 μM deciding of efficient substrate cleavage by effector caspases. At high XIAP concentrations, substrate cleavage is potently blocked. (**B**) Comparison of XIAP expression levels. Western blot comparing XIAP expression levels of HeLa cells infected with AdV-LacZ or AdV-XIAP. β-Actin served as loading control. (**C**) Mitochondrial depolarisation and subsequent effector caspase activation are shown for a representative HeLa cell infected with AdV-XIAP (m.o.i. 100) and treated with 1 μM STS. Mitochondrial depolarisation is shown as a decrease in TMRM fluorescence. Effector caspase activation was detected by an increase in the CFP/YFP emission ratio owing to proteolytic cleavage of a CFP-DEVD-YFP fusion protein. Scale bar = 10 μm. Time stamps show the time after stimulus addition. (**D**) Model-calculated substrate cleavage kinetics around 4.5-fold XIAP overexpression (0.26–0.30 μM). (**E**) Submaximal substrate cleavage upon XIAP overexpression. Microscopy images were quantitatively analysed and traces for three XIAP overexpressing HeLa cells treated with 1 μM STS are shown. Traces were synchronised to the time point of depolarisation for comparability to the model predictions in (D). (**F**) Delay between mitochondrial depolarisation and effector caspase activation. Data from $n=32$ (AdV-LacZ) and 41 (AdV-XIAP) cells are shown as median ± first and third quartiles, respectively. Noninfected cells served as controls ($n=16$). XIAP overexpression significantly delayed effector caspase activation after MOMP when compared to LacZ-infected cells ($P=3.6\times10^{-10}$; Mann–Whitney *U*-test). Model predictions (Calc) are shown as comparison. (**G**) Evaluation of substrate cleavage kinetics of single cells. CFP/YFP ratio traces for single cells were fitted with a sigmoid Boltzmann function. d*t* determines the width of the turnover of the sigmoid function. Data from $n=27$ (AdV-LacZ) and $n=41$ (AdV-XIAP) cells are shown as median ± first and third quartiles. Noninfected cells served as controls ($n=19$). XIAP overexpression significantly slowed down substrate cleavage when compared to LacZ-infected cells ($P=9.1\times10^{-6}$; independent samples *t*-test). Model predictions (Calc) are shown as comparison.

©2006 European Molecular Biology Organization

or population-based studies (that lack temporal resolution and are sensitive to asynchrony in apoptosis commitment) (Stucki and Simon, 2005; Bagci *et al*, 2006). This was achieved by comparing the outputs of the systems biology approach directly with a similar output that could be detected in single-cell analyses. The computational model also en-

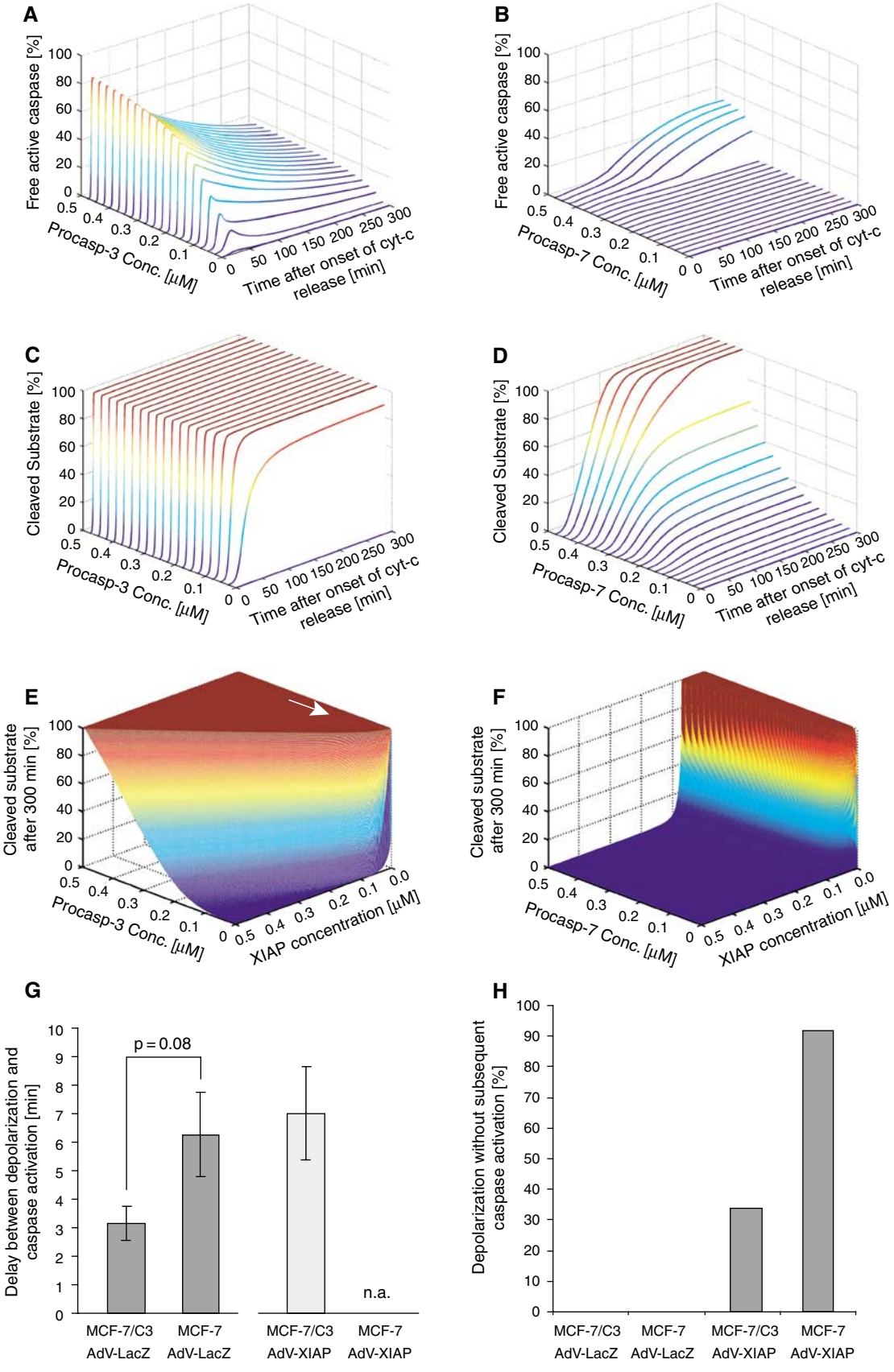

©2006 European Molecular Biology Organization

abled us to calculate simultaneously the temporal profiles of the 19 proteins and protein complexes involved in this process. Currently, this can only be achieved by a systems approach, as single-cell imaging set ups are confined to monitor only a limited number of biological processes in a single experiment.

Although the model was able to explain cellular all-or-none responses and to differentiate between key processes and redundant processes, the current model still has limitations. The most important limitation is that it allows for a temporal simulation, but that spatial effects such as intracellular gradients and protein redistributions were omitted from calculations. In epithelial cells such as HeLa cells, diffusion processes would equalise concentration ramps within seconds, whereas signalling occurred in a time frame of minutes. Diffusion processes can therefore be largely ignored. However, spatial analysis of signal progression might become important for large or polarised cells such as neurons, megakaryocytes or myotubes and would require the extension of the current model to a spatiotemporal simulation. Indeed, locally restricted effector caspase activation has been reported to occur during neuronal injury after cerebral ischaemia and during sperm and macrophage cell differentiation (Sordet *et al*, 2002; Arama *et al*, 2003). In these scenarios, caspase activity might be confined to distinct subcellular compartments or subcellular organelles, and a propagation of death signals from one compartment to the next might be subject to additional control steps.

It is also important to note that the model predicts effector caspase activation and substrate cleavage but not explicitly cell death or survival. Other routes to cell death have been described that compensate for a lack of effector caspase activation. Mitochondrial dysfunction secondary to MOMP can lead to impaired respiration and ATP production, and caspase-independent cell death after MOMP can be partially rescued by the supply of glucose (Lang-Rollin *et al*, 2003). MOMP is also able to trigger a Bcl-2-sensitive, caspase-independent cell death by autophagy (Tolkovsky *et al*, 2002; Lang-Rollin *et al*, 2003). Even though these alternative routes to cell death exist, the ability to induce apoptosome-dependent caspase activation is essential during development. In mice lacking core components of this signalling system, neurons are incapable of dying through alternative pathways, and animals display nervous system hyperplasia and are not viable (Kuida *et al*, 1996, 1998; Cecconi *et al*, 1998). In the adult system, rapid effector caspase activation may likewise be required for an efficient removal of defective cells by phagocytosis (Lauber *et al*, 2004), thereby preventing tissue inflammation and promoting tissue regeneration. Hence, the ability of cells to undergo rapid effector caspase activation may be important both during development and in the adult organism. Our study provides a comprehensive explanation for this important phenomenon and its control by XIAP.

Materials and methods

Materials

Embryo-tested mineral oil was from Sigma. STS was from Alexis (Grünberg, Germany). TMRM was from MobiTec (Göttingen, Germany).

Cell culture and transfection

All cells were cultured in RPMI 1640 medium (Sigma) supplemented with penicillin (100 U/ml), streptomycin (100 μg/ml) and 10% fetal calf serum (PAA, Cölbe, Germany). Cells were transfected with 0.6 μg of plasmid DNA (pmyc-CFP-DEVD-YFP; Tyas *et al*, 2000), and 6 μl Lipofectamin 2000 (Invitrogen) per milliliter of serum-free medium at 37°C for 4 h. Generation and characterisation of MCF-7 cells and HeLa cells stably expressing a CFP-DEVD-YFP fusion protein have been previously described (Rehm *et al*, 2002).

Adenoviral infections

AdV vectors to express β-galactosidase or XIAP were a gift from Dr JB Schulz (University of Goettingen, Germany). Vector generation has been described previously (Eberhardt *et al*, 2000). Cells were washed with PBS and infected at m.o.i. of 100 in serum-free medium for 3 h and subsequently cultured in full growth medium. Experiments were carried out 24 h after infection.

Western blotting

Equal amounts of protein (30 μg) were loaded onto sodium dodecyl sulphate (SDS)–PAGE gel (10%). Proteins were separated at 130 V for 1.5 h and blotted to nitrocellulose membranes (Protean BA 83; Schleicher & Schuell, Germany) in transfer buffer (25 mM Tris, 192 mM glycine, 20% methanol (v/v) and 0.01% SDS) at 18 V for 60 min. Blots were blocked with 5% nonfat dry milk in Tris-buffered saline with 0.1% Tween (TBST) (15 mM Tris–HCl pH 7.5, 200 mM NaCl and 0.1% Tween-20) at room temperature for 2 h. Membranes were incubated with a mouse monoclonal anti-XIAP antibody (1:2000, BD), a rabbit polyclonal anti-caspase-3 antibody (1:1000, Santa Cruz) or a mouse monoclonal anti-β-actin antibody (1:5000, Sigma). Membranes were washed with TBST three times for 10 min and incubated with anti-mouse or anti-rabbit peroxidase-conjugated secondary antibodies (1:4000, Jackson ImmunoResearch, PA, USA) for 1 h. Blots were washed and developed using an enhanced chemiluminescence detection reagent (Amersham, UK).

Time-lapse microscopy and digital imaging

Cells were equilibrated with 30 nM TMRM in *N*-2-hydroxyl piperazine-*N*′-2-ehane sulfonic acid-buffered medium (10 mM; pH 7.4), covered with mineral oil, and placed in heated (37°C)

Figure 6 Role of caspase-3 feedback signalling in all-or-none caspase activation. (**A–F**) Model responses for apoptotic signalling with (A, C, E) or without (B, D, F) caspase-3. Upon loss of caspase-3, caspase-7 served as the central effector caspase. (A, B) Temporal effector caspase activation profiles upon varying the initial procaspase concentrations. (A) Caspase-3 activation is rapid and results in a sharp peak of free active caspase-3 (caspase-3 that is not inhibited by XIAP or BIR1-2). A high percentage of the overall amount of procaspase gets activated. (B) In the absence of caspase-3, caspase-7 activation is slow, does not exceed ~35% of the initial amount of procaspase-7 and is not detectable at concentrations below ~0.35 μM. (C, D) Temporal profiles of substrate cleavage upon varying the initial procaspase concentrations. (C) In caspase-3-expressing cells, small concentrations of procaspase-3 are sufficient to result in complete substrate cleavage whereas (D) considerably higher amounts of procaspase-7 are needed for complete substrate cleavage. (E, F) Substrate cleavage as a consequence of the procaspase/XIAP balance. (E) Only on substantial overexpression of XIAP substrate cleavage can be inhibited in presence of caspase-3, whereas a slight overexpression of XIAP in caspase-3-deficient cells results in a complete inhibition of substrate cleavage (F). Arrow points at the standard conditions in HeLa cells. (G–H) Experimental results from single-cell analyses of caspase-3-deficient MCF-7 cells. (**G**) FRET substrate cleavage is significantly delayed upon loss of caspase-3. Data from $n = 26$, 23 and 10 cells are shown as mean ± s.e.m. MCF-7 cells show a delay in substrate cleavage following depolarisation ($P = 0.08$; *U*-test). Overexpression of XIAP in MCF-7/C3 cells delays substrate cleavage to a similar extent ($P = 0.04$; *U*-test). NA, not applicable. (**H**) MCF-7/caspase-3 and MCF-7 cells infected with either β-galactosidase or XIAP expression adenoviruses (AdV-LacZ; AdV-XIAP; m.o.i. 100) were treated with 1 μM STS. Cells not showing effector caspase activity following mitochondrial depolarisation were quantified.

©2006 European Molecular Biology Organization

incubation chambers that were mounted on the microscope stages. Apoptosis was induced with 1 μM STS.

The epifluorescence microscope used was a Nikon TE 300 with a ×40 S-Fluor oil objective (Nikon, Germany), equipped with a polychroic mirror and filter wheels in the excitation and emission light paths containing the appropriate filter sets (Rehm *et al*, 2003). Images were recorded using a cooled CCD camera (Spot RT SE6, Diagnostic Instruments). The imaging setup was controlled by MetaMorph software (Universal Imaging, PA, USA).

The confocal microscope used was a Zeiss LSM 500 META inverted microscope (Carl Zeiss, Germany) attached to a confocal laser scanning unit equipped with a 405-nm diode laser, 488-nm argon laser and a 543-nm helium/neon laser. Using a ×63 oil fluorescence objective, CFP, FRET, YFP and TMRM fluorescence were monitored and quantified confocally using optimised filter and mirror sets. The membrane-permeant, cationic probe TMRM distributes across cellular membranes according to the Nernstian equation. TMRM has little effects on the respiratory chain activity at the concentration used in the present study (30 nM).

Kinetics of $\Delta\Psi_M$ depolarisation and FRET disruption

For analysis of $\Delta\Psi_M$ kinetics in single cells, the fluorescent mitochondrial regions were segmented from the cytoplasmic and nucleus regions. After background subtraction, the average fluorescence intensity per pixel was calculated. This value resembles the concentration of TMRM inside mitochondria (Dussmann *et al*, 2003).

Caspase cleavage kinetics was detected at the single-cell level by FRET analysis. Images were processed using MetaMorph software. CFP/YFP emission ratio traces were obtained by dividing the average fluorescence intensity values of single cells after background subtraction. Plots were scaled and fitted with the sigmoid Boltzmann function $y=(A1-A2)/(1+\exp((x-x0)/dt))+A2$ with dt determining the width of the turnover, $A1$ the minimum, $A2$ the maximum and $x0$ the time when the turning point of the function is reached. Data for dt were analysed for significance statistically.

The percentage of FRET substrate cleavage was determined by calibrating changes in the CFP/YFP emission ratios. To account for possible bleaching throughout the measurement, ratios were corrected for CFP/YFP changes in nonapoptotic control cells. As the FRET substrate is fully cleaved in parental apoptotic cells (Rehm *et al*, 2002), the mean CFP/YFP emission ratio change in parental apoptotic control cells was equated with 100% substrate cleavage.

Statistics

For statistical comparison, *t*-test or analysis of variance and subsequent Tukey's test were employed. Data that were not standard deviated were analysed by Mann–Whitney *U*-test. *P*-values smaller than 0.05 were considered to be statistically significant.

Computational modelling

The reaction network was designed on the basis of mass action kinetics. As model trigger, cyt-*c*-dependent apoptosome formation and mitochondrial Smac release were described by an exponential saturation function resembling experimental kinetic data. All processes and reactions described in Figure 1A were implemented in a MATLAB-based script using an adaptive step Runge–Kutta ordinary differential equation (ODE) solver (Gear74). The model is comprised of 53 reactions, 19 reaction partners and 75 reaction parameters. Parameters were obtained from the literature or by independent analysis of the authors (see Supplementary data 1 and 2). The model's output function (resulting substrate cleavage) has been calculated by direct integration of the effector caspase activation profile. Modelling was performed over a time period of 24 h (resembling the HeLa cell cycle duration). Graphs display significant changes within the time stated on the respective axes. No significant changes occurred beyond the time periods depicted in the graphs. Concentration thresholds were based on the time period of 24 h. A full documentation of the model can be found online as Supplementary data 1. The model is provided as a webservice and MATLAB script at http://systemsbiology.rcsi.ie.

Supplementary data

Supplementary data are available at *The EMBO Journal* Online (http://www.embojournal.org).

Acknowledgements

This research was supported by grants from Science Foundation Ireland to JHMP (03/RP1/B344 and 03/RP1/B344S) and MR (05/RFP/BIM056), and by Siemens Research Ireland. We thank Drs J Schulz (University of Goettingen) and X Wang (University of Texas) and Ms P Völler (VU Amsterdam) for supply of adenoviral vectors and recombinant proteins, and Drs C Concannon, G Cohen, D Green and S Martin for their constructive criticisms and helpful discussions.

References

Arama E, Agapite J, Steller H (2003) Caspase activity and a specific cytochrome *C* are required for sperm differentiation in *Drosophila*. *Dev Cell* **4:** 687–697

Arnoult D, Gaume B, Karbowski M, Sharpe JC, Cecconi F, Youle RJ (2003) Mitochondrial release of AIF and EndoG requires caspase activation downstream of Bax/Bak-mediated permeabilization. *EMBO J* **22:** 4385–4399

Arnt CR, Chiorean MV, Heldebrant MP, Gores GJ, Kaufmann SH (2002) Synthetic Smac/DIABLO peptides enhance the effects of chemotherapeutic agents by binding XIAP and cIAP1 *in situ*. *J Biol Chem* **277:** 44236–44243

Bagci EZ, Vodovotz Y, Billiar TR, Ermentrout GB, Bahar I (2006) Bistability in apoptosis: roles of bax, bcl-2, and mitochondrial permeability transition pores. *Biophys J* **90:** 1546–1559

Bentele M, Lavrik I, Ulrich M, Stosser S, Heermann DW, Kalthoff H, Krammer PH, Eils R (2004) Mathematical modeling reveals threshold mechanism in CD95-induced apoptosis. *J Cell Biol* **166:** 839–851

Cecconi F, Alvarez-Bolado G, Meyer BI, Roth KA, Gruss P (1998) Apaf1 (CED-4 homolog) regulates programmed cell death in mammalian development. *Cell* **94:** 727–737

Clarke MC, Savill J, Jones DB, Noble BS, Brown SB (2003) Compartmentalized megakaryocyte death generates functional platelets committed to caspase-independent death. *J Cell Biol* **160:** 577–587

Deveraux QL, Reed JC (1999) IAP family proteins—suppressors of apoptosis. *Genes Dev* **13:** 239–252

Du C, Fang M, Li Y, Li L, Wang X (2000) Smac, a mitochondrial protein that promotes cytochrome *c*-dependent caspase activation by eliminating IAP inhibition. *Cell* **102:** 33–42

Dussmann H, Rehm M, Kogel D, Prehn JH (2003) Outer mitochondrial membrane permeabilization during apoptosis triggers caspase-independent mitochondrial and caspase-dependent plasma membrane potential depolarization: a single-cell analysis. *J Cell Sci* **116:** 525–536

Eberhardt O, Coelln RV, Kugler S, Lindenau J, Rathke-Hartlieb S, Gerhardt E, Haid S, Isenmann S, Gravel C, Srinivasan A, Bahr M, Weller M, Dichgans J, Schulz JB (2000) Protection by synergistic effects of adenovirus-mediated X-chromosome-linked inhibitor of apoptosis and glial cell line-derived neurotrophic factor gene transfer in the 1-methyl-4-phenyl-1,2,3,6-tetrahydropyridine model of Parkinson's disease. *J Neurosci* **20:** 9126–9134

Eissing T, Conzelmann H, Gilles ED, Allgower F, Bullinger E, Scheurich P (2004) Bistability analyses of a caspase activation model for receptor-induced apoptosis. *J Biol Chem* **279:** 36892–36897

Goldstein JC, Munoz-Pinedo C, Ricci JE, Adams SR, Kelekar A, Schuler M, Tsien RY, Green DR (2005) Cytochrome *c* is released in a single step during apoptosis. *Cell Death Differ* **12:** 453–462

Goldstein JC, Waterhouse NJ, Juin P, Evan GI, Green DR (2000) The coordinate release of cytochrome *c* during apoptosis is rapid, complete and kinetically invariant. *Nat Cell Biol* **2:** 156–162

Harlin H, Reffey SB, Duckett CS, Lindsten T, Thompson CB (2001) Characterization of XIAP-deficient mice. *Mol Cell Biol* **21:** 3604–3608

 ©2006 European Molecular Biology Organization

Janicke RU, Ng P, Sprengart ML, Porter AG (1998a) Caspase-3 is required for alpha-fodrin cleavage but dispensable for cleavage of other death substrates in apoptosis. *J Biol Chem* **273:** 15540–15545

Janicke RU, Sprengart ML, Wati MR, Porter AG (1998b) Caspase-3 is required for DNA fragmentation and morphological changes associated with apoptosis. *J Biol Chem* **273:** 9357–9360

Kashkar H, Haefs C, Shin H, Hamilton-Dutoit SJ, Salvesen GS, Kronke M, Jurgensmeier JM (2003) XIAP-mediated caspase inhibition in Hodgkin's lymphoma-derived B cells. *J Exp Med* **198:** 341–347

Kuida K, Haydar TF, Kuan CY, Gu Y, Taya C, Karasuyama H, Su MS, Rakic P, Flavell RA (1998) Reduced apoptosis and cytochrome *c*-mediated caspase activation in mice lacking caspase 9. *Cell* **94:** 325–337

Kuida K, Zheng TS, Na S, Kuan C, Yang D, Karasuyama H, Rakic P, Flavell RA (1996) Decreased apoptosis in the brain and premature lethality in CPP32-deficient mice. *Nature* **384:** 368–372

Lang-Rollin IC, Rideout HJ, Noticewala M, Stefanis L (2003) Mechanisms of caspase-independent neuronal death: energy depletion and free radical generation. *J Neurosci* **23:** 11015–11025

Lauber K, Blumenthal SG, Waibel M, Wesselborg S (2004) Clearance of apoptotic cells: getting rid of the corpses. *Mol Cell* **14:** 277–287

Li L, Thomas RM, Suzuki H, De Brabander JK, Wang X, Harran PG (2004) A small molecule Smac mimic potentiates TRAIL- and TNFalpha-mediated cell death. *Science* **305:** 1471–1474

Li P, Nijhawan D, Budihardjo I, Srinivasula SM, Ahmad M, Alnemri ES, Wang X (1997) Cytochrome *c* and dATP-dependent formation of Apaf-1/caspase-9 complex initiates an apoptotic protease cascade. *Cell* **91:** 479–489

MacFarlane M, Merrison W, Bratton SB, Cohen GM (2002) Proteasome-mediated degradation of Smac during apoptosis: XIAP promotes Smac ubiquitination *in vitro*. *J Biol Chem* **277:** 36611–36616

Meier P, Finch A, Evan G (2000) Apoptosis in development. *Nature* **407:** 796–801

Murphy BM, O'Neill AJ, Adrain C, Watson RW, Martin SJ (2003) The apoptosome pathway to caspase activation in primary human neutrophils exhibits dramatically reduced requirements for cytochrome *C*. *J Exp Med* **197:** 625–632

Okada H, Suh WK, Jin J, Woo M, Du C, Elia A, Duncan GS, Wakeham A, Itie A, Lowe SW, Wang X, Mak TW (2002) Generation and characterization of Smac/DIABLO-deficient mice. *Mol Cell Biol* **22:** 3509–3517

Potts PR, Singh S, Knezek M, Thompson CB, Deshmukh M (2003) Critical function of endogenous XIAP in regulating caspase activation during sympathetic neuronal apoptosis. *J Cell Biol* **163:** 789–799

Rehm M, Dussmann H, Janicke RU, Tavare JM, Kogel D, Prehn JH (2002) Single-cell fluorescence resonance energy transfer analysis demonstrates that caspase activation during apoptosis is a rapid process. Role of caspase-3. *J Biol Chem* **277:** 24506–24514

Rehm M, Dussmann H, Prehn JH (2003) Real-time single cell analysis of Smac/DIABLO release during apoptosis. *J Cell Biol* **162:** 1031–1043

Ricci JE, Munoz-Pinedo C, Fitzgerald P, Bailly-Maitre B, Perkins GA, Yadava N, Scheffler IE, Ellisman MH, Green DR (2004) Disruption of mitochondrial function during apoptosis is mediated by caspase cleavage of the p75 subunit of complex I of the electron transport chain. *Cell* **117:** 773–786

Slee EA, Harte MT, Kluck RM, Wolf BB, Casiano CA, Newmeyer DD, Wang HG, Reed JC, Nicholson DW, Alnemri ES, Green DR, Martin SJ (1999) Ordering the cytochrome *c*-initiated caspase cascade: hierarchical activation of caspases-2, -3, -6, -7, -8, and -10 in a caspase-9-dependent manner. *J Cell Biol* **144:** 281–292

Sordet O, Rebe C, Plenchette S, Zermati Y, Hermine O, Vainchenker W, Garrido C, Solary E, Dubrez-Daloz L (2002) Specific involvement of caspases in the differentiation of monocytes into macrophages. *Blood* **100:** 4446–4453

Srinivasula SM, Hegde R, Saleh A, Datta P, Shiozaki E, Chai J, Lee RA, Robbins PD, Fernandes-Alnemri T, Shi Y, Alnemri ES (2001) A conserved XIAP-interaction motif in caspase-9 and Smac/DIABLO regulates caspase activity and apoptosis. *Nature* **410:** 112–116

Stucki JW, Simon HU (2005) Mathematical modeling of the regulation of caspase-3 activation and degradation. *J Theor Biol* **234:** 123–131

Sun XM, Butterworth M, MacFarlane M, Dubiel W, Ciechanover A, Cohen GM (2004) Caspase activation inhibits proteasome function during apoptosis. *Mol Cell* **14:** 81–93

Suzuki Y, Nakabayashi Y, Takahashi R (2001) Ubiquitin-protein ligase activity of X-linked inhibitor of apoptosis protein promotes proteasomal degradation of caspase-3 and enhances its anti-apoptotic effect in Fas-induced cell death. *Proc Natl Acad Sci USA* **98:** 8662–8667

Tafani M, Minchenko DA, Serroni A, Farber JL (2001) Induction of the mitochondrial permeability transition mediates the killing of HeLa cells by staurosporine. *Cancer Res* **61:** 2459–2466

Tamm I, Kornblau SM, Segall H, Krajewski S, Welsh K, Kitada S, Scudiero DA, Tudor G, Qui YH, Monks A, Andreeff M, Reed JC (2000) Expression and prognostic significance of IAP-family genes in human cancers and myeloid leukemias. *Clin Cancer Res* **6:** 1796–1803

Tolkovsky AM, Xue L, Fletcher GC, Borutaite V (2002) Mitochondrial disappearance from cells: a clue to the role of autophagy in programmed cell death and disease? *Biochimie* **84:** 233–240

Tyas L, Brophy VA, Pope A, Rivett AJ, Tavare JM (2000) Rapid caspase-3 activation during apoptosis revealed using fluorescence-resonance energy transfer. *EMBO rep* **1:** 266–270

Varnes ME, Chiu SM, Xue LY, Oleinick NL (1999) Photodynamic therapy-induced apoptosis in lymphoma cells: translocation of cytochrome *c* causes inhibition of respiration as well as caspase activation. *Biochem Biophys Res Commun* **255:** 673–679

Vaughan AT, Betti CJ, Villalobos MJ (2002) Surviving apoptosis. *Apoptosis* **7:** 173–177

Verhagen AM, Ekert PG, Pakusch M, Silke J, Connolly LM, Reid GE, Moritz RL, Simpson RJ, Vaux DL (2000) Identification of DIABLO, a mammalian protein that promotes apoptosis by binding to and antagonizing IAP proteins. *Cell* **102:** 43–53

Weber GF, Menko AS (2005) The canonical intrinsic mitochondrial death pathway has a non-apoptotic role in signaling lens cell differentiation. *J Biol Chem* **280:** 22135–22145

Wilkinson JC, Cepero E, Boise LH, Duckett CS (2004) Upstream regulatory role for XIAP in receptor-mediated apoptosis. *Mol Cell Biol* **24:** 7003–7014

Wu G, Chai J, Suber TL, Wu JW, Du C, Wang X, Shi Y (2000) Structural basis of IAP recognition by Smac/DIABLO. *Nature* **408:** 1008–1012

Yoshida H, Kong YY, Yoshida R, Elia AJ, Hakem A, Hakem R, Penninger JM, Mak TW (1998) Apaf1 is required for mitochondrial pathways of apoptosis and brain development. *Cell* **94:** 739–750

Yuan J, Yankner BA (2000) Apoptosis in the nervous system. *Nature* **407:** 802–809

Zou H, Henzel WJ, Liu X, Lutschg A, Wang X (1997) Apaf-1, a human protein homologous to C. elegans CED-4, participates in cytochrome *c*-dependent activation of caspase-3. *Cell* **90:** 405–413

Zou H, Yang R, Hao J, Wang J, Sun C, Fesik SW, Wu JC, Tomaselli KJ, Armstrong RC (2003) Regulation of the Apaf-1/caspase-9 apoptosome by caspase-3 and XIAP. *J Biol Chem* **278:** 8091–8098

©2006 European Molecular Biology Organization